

# Distinction of different two-photon transition pathways by spatial coherent control

Dewen Cao<sup>1,2</sup>, Yaxiong Wang<sup>1,2</sup>, Shouzhi Li<sup>1,2</sup>, Ling Yang<sup>1,2</sup>, Shuang Feng<sup>1,2,3</sup>, Gao Fang<sup>1</sup>

1. Institute of Intelligent Machines, Chinese Academy of Sciences, Hefei, Anhui 230031, China

2. Department of Automation, University of Science and Technology of China, Hefei, Anhui 230026, China

3. Department of Mechanical Engineering, Anhui Polytechnic University, Wuhu, Anhui 241000, China

E-mail: gaofang@iim.ac.cn

**Abstract:** The spatial coherent control of resonant two-photon transitions in atomic rubidium using counter-propagating ultra-short laser pulses is investigated in this work. There are two transition pathways involved in the spatial excitation pattern. A special pulse shaping scheme is designed to distinguish their individual contribution. The scheme consists of a  $\pi$ -step function flipping at the poles and zeros of the transition amplitude function and two segmented linear function with different slopes, and it can make the desired transition pathway dominate at the assigned spatial position. The simulations show that our scheme is quite effective compared to the previous single linear shaping scheme.

**Key Words:** spatial coherent control, pathway distinction, resonant two-photon transitions, pulse shaping

## 1 Introduction

Quantum coherent control via light-matter interactions can steer the quantum dynamics in atomic and molecular systems. In early experiments, shaped ultrashort laser pulses [1] were employed to control the quantum processes. Two-photon absorption (TPA) is one fundamental quantum process and numerous control schemes have been proposed to achieve optimal enhancement and selective excitation. The simplest case is one two-photon transition pathway in a three-level quantum system [2–6]. When there are two pathways in a four-level quantum system, the quantum coherent control and pathway manipulation can be further investigated by considering the interference between the two pathways [7–10]. Spatial coherent control can induce different interference patterns in space, and thus has many applications in physics [11–13].

Itan Barmes introduced the spatial degree of freedom into the TPA control by using a pair of counter-propagating ultrashort frequency combs [14, 15], and they demonstrated spatially selective excitation of individual species in a multi-component gas mixture for non-resonant TPA. Subsequently, Dirk Boonzajer [16] and Woojun Lee [17] investigated the spatial coherent control for the resonant TPA of  $5S_{1/2} \rightarrow 5P_{3/2} \rightarrow 5D$  in atomic rubidium.

In this paper, we described a spatial coherent control scheme for the distinction of two resonant TPA pathways in atomic rubidium, which are  $5S_{1/2} \rightarrow 5P_{3/2} \rightarrow 5D$  and  $5S_{1/2} \rightarrow 5P_{1/2} \rightarrow 5D$ . In Section 2, the spatial coherent control experiment set-up and TPA theoretical model induced by the counter-propagating ultrashort pulse pairs are introduced. Section 3 gives several phase shaping schemes and the simulations, and the scheme containing double linear

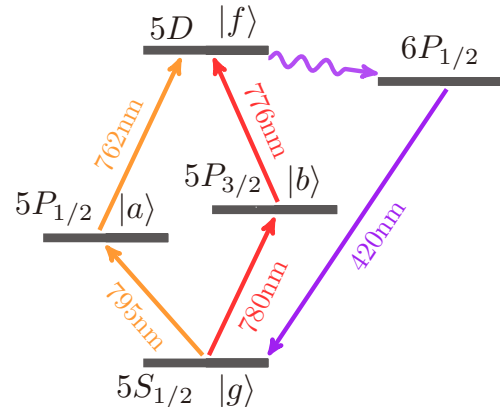


Figure 1: (Color online) The energy-level diagram of atomic rubidium. The atoms are excited from the ground state  $5S_{1/2}$  ( $|g\rangle$ ) to the final state  $5D$  ( $|f\rangle$ ) through the two intermediate states  $5P_{1/2}$  ( $|a\rangle$ ) and  $5P_{3/2}$  ( $|b\rangle$ ), respectively. There are two two-photon transition pathways: (i) pathway 1,  $|g\rangle \rightarrow |a\rangle \rightarrow |f\rangle$  and (ii) pathway 2,  $|g\rangle \rightarrow |b\rangle \rightarrow |f\rangle$ . The pulse spectrum is centered on the two-photon transition frequency ( $\omega_{fg}/2$ ). Fluorescence decayed from the  $6P$  state at 420 nm is used to detect the excited state population.

functions can distinguish the pathway amplitude quite well. The conclusion is given in Section 4.

## 2 Theoretical considerations

The spectral spatial coherent control of atomic rubidium (level diagrams are presented in Fig. 1) with counter-propagating ultrashort pulse pairs is considered in this work. The layout of the experimental setup is shown in Fig. 2. Briefly, femtosecond optical pulses are shaped in a 4f-configuration zero-dispersion shaper and the phases are controlled by a spatial light modulator. The shaped pulse are firstly focused in a rubidium vapour cell and then reflected back by a mirror, so each counter-propagating laser pulse collides with the next pulse in the vapor cell. The excited state population is proportional to 420 nm fluorescence de-

The authors acknowledge support by the National Natural Science Foundation of China (Grants No. 61203061, No. 61403362, 61374091, and No. 61473199). F. Shuang thanks the Leader talent plan of the Universities in Anhui Province and the CAS Interdisciplinary Innovation Team of the Chinese Academy of Sciences for financial support. The authors gratefully acknowledge the large contribution of Jaewook Ahn, Woojun Lee, Minhyuk Kim, Department of Physics, Korea Advanced Institute of Science and Technology, Republic of Korea.

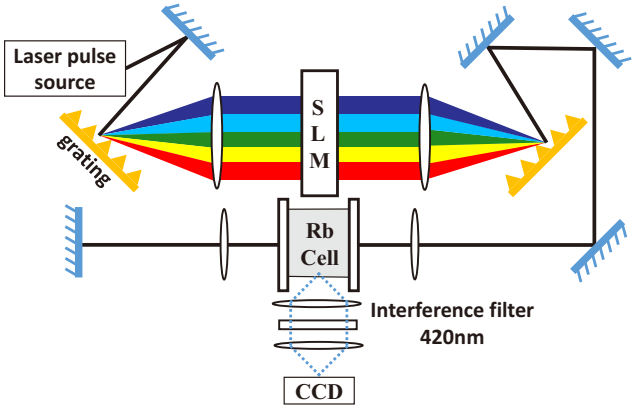


Figure 2: (Color online) Schematic set-up of the spatial coherent control experiment. The pulses are shaped by the spatial light modulator (SLM). Every two counter-propagating pulses collide in the vapour cell and excite the two-photon transitions. The fluorescence pattern is imaged by an charge-coupled device camera.

cayed from the  $6P$  state, which is monitored by a charge-couple device (CCD) camera.

According to the second-order time dependent perturbation theory, the two-photon transitions amplitude  $U(t)$  induced by a weak laser field  $\varepsilon(t)$  is

$$U(z, t) = -\frac{1}{\hbar^2} \sum_{n=a,b} \mu_{fn} \mu_{ng} \int_{-\infty}^t \int_{-\infty}^{t_1} \varepsilon(z, t_1) \varepsilon(z, t_2) \times e^{i\omega_{fn} t_1} e^{i\omega_{ng} t_2} dt_2 dt_1, \quad (1)$$

where  $\mu_{fn}$  and  $\mu_{ng}$  are the transition dipoles, and  $\omega_{ij} = (E_i - E_j)/\hbar$  are the frequency difference between the state  $|i\rangle$  and  $|j\rangle$ . The summation is performed over all possible intermediate states. The electric field is  $\varepsilon(z, t) = \varepsilon_1(z, t) + \varepsilon_2(z, t)$ , in which  $\varepsilon_1(z, t)$  and  $\varepsilon_2(z, t)$  propagate along the  $+z$  and  $-z$  directions respectively.

With the Fourier transformation, the final amplitude can be written in the frequency domain when the pulse is over

(i.e.,  $t \rightarrow \infty$ ).

$$U(z) = \sum_{n=a,b} i \frac{\mu_{fn} \mu_{ng}}{\hbar^2} \left[ i\pi E(\omega_{ng}) E(\omega_{fn}) + \wp \int_{-\infty}^{\infty} \frac{E(\omega) E(\omega_{fg} - \omega)}{\omega_{ng} - \omega} d\omega \right], \quad (2)$$

where  $E(\omega)$  is the Fourier transform of  $\varepsilon(t)$ .

For convenience, we define  $\hat{\omega} = \omega_{fg} - \omega$ ,  $v_n = \mu_{fn} \mu_{ng} / \hbar^2$  and  $\omega_0 = \omega_{fg}/2$ . Then the TPA amplitudes are can be rewritten as

$$U_r^{(n)}(z) = U_r^{(n)}(z) + U_{nr}^{(n)}(z), \quad (3)$$

$$U(z) = \sum_{n=a,b} \left[ U_r^{(n)}(z) + U_{nr}^{(n)}(z) \right], \quad (4)$$

with

$$U_r^{(n)}(z) = -\pi v_n E(\omega_{ng}) E(\omega_{fn}), \quad (5)$$

$$U_{nr}^{(n)}(z) = iv_n \wp \int_{\omega_0}^{\infty} \frac{(\omega_{fn} - \omega_{ng}) E(\omega) E(\hat{\omega})}{(\omega - \omega_{ng})(\omega - \omega_{fn})} d\omega. \quad (6)$$

Here  $U_r^{(n)}(z)$  denotes the resonant part of each pathway amplitude, which only dependents on the resonance frequency;  $U_{nr}^{(n)}(z)$  denotes the non-resonant part, which considers the contributions of the other spectral components.

$$E(\omega) = E_1(\omega) e^{-i\omega z/c} + E_2(\omega) e^{i\omega z/c}, \quad (7)$$

where  $E_1(\omega) = f[\varepsilon_1(0, t)]$  and  $E_2(\omega) = f[\varepsilon_2(0, t)]$  are, respectively, the Fourier transformation of electric field, and  $c$  is the speed of light.

Since the counter-propagating pulses are split from the same single laser pulse, they have the same spectral amplitude function  $A(\omega)$  and phase function  $\phi(\omega)$ ,

$$E_1(\omega) = E_2(\omega) = A(\omega) e^{i\phi(\omega)}. \quad (8)$$

Thus the resonant and non-resonant terms can be written as

$$U_r(z) = \sum_{n=a,b} U_r^{(n)}(z) = -4\pi \sum_{n=a,b} v_n A(\omega_{ng}) A(\omega_{fn}) e^{i\phi(\omega_{ng}) + i\phi(\omega_{fn})} \cos\left(\frac{\omega_{ng} z}{c}\right) \cos\left(\frac{\omega_{fn} z}{c}\right), \quad (9)$$

$$U_{nr}(z) = \sum_{n=a,b} U_{nr}^{(n)}(z) = 4i \int_{\omega_0}^{\infty} A(\omega) A(\hat{\omega}) e^{i\phi(\omega) + i\phi(\hat{\omega})} \cos\left(\frac{\hat{\omega} z}{c}\right) \cos\left(\frac{\omega z}{c}\right) f(\omega) d\omega, \quad (10)$$

where

$$f(\omega) = \frac{(\omega - \omega_{fo})(\omega - \omega_{og})(\omega_{fa} - \omega_{ag})(\omega_{fb} - \omega_{bg})}{(\omega - \omega_{fa})(\omega - \omega_{fb})(\omega - \omega_{ag})(\omega - \omega_{bg})},$$

$$\omega_{fo} = \omega_0 + \frac{\gamma}{2} \sqrt{(\omega_{fa} - \omega_{ag})(\omega_{fa} - \omega_{ag})},$$

$$\omega_{og} = \omega_0 - \frac{\gamma}{2} \sqrt{(\omega_{fa} - \omega_{ag})(\omega_{fa} - \omega_{ag})},$$

$$\gamma = \sqrt{\frac{\beta + \alpha}{1 + \alpha\beta}}, \quad \alpha = \frac{v_b}{v_a}, \quad \beta = \frac{\omega_{fb} - \omega_{bg}}{\omega_{fa} - \omega_{ag}}.$$

The  $f(\omega)$  changes the sign at the poles (i.e.,  $\omega_{fn}$  and  $\omega_{ng}$ ) and zeros (i.e.,  $\omega_{fo}$  and  $\omega_{og}$ ) [10]. By flipping the phases at these characteristic frequencies, we can avoid the destructive interferences.

At a certain spatial position  $z$ , the trigonometric factor (i.e., cosine function) of the non-resonant integral  $U_{nr}(z)$  leads to a period of  $\pi c/z$  for  $\omega$ . When the phase item (i.e.,  $e^{i\phi(\omega) + i\phi(\hat{\omega})}$ ) is also set as a periodic function with the same period of  $\pi c/z$ , the maximal transition amplitude will be

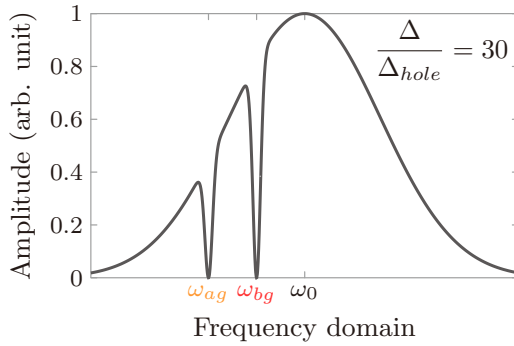


Figure 3: (Color online) The amplitude function  $A(\omega)$  vs  $\omega$  centered at  $\omega_0$ . There are two holes located at the resonance frequencies  $\omega_{ag}$  and  $\omega_{bg}$ , respectively. Here  $\Delta/\Delta_{hole} = 30$  is used.

achieved. As the cosine is an even function, the spatial symmetry relationships are obtained as  $U(z) = U(-z)$  and  $U^{(n)}(z) = U^{(n)}(-z)$ .

### 3 Results and discussion

To involve the quantum interference between pathways, laser pulses with a wide spectral bandwidth (full width at half maximum) about 45 nm are employed. We use a Gaussian amplitude function  $A(\omega)$  with two holes around the two resonant frequencies  $\omega_{ag}$  and  $\omega_{bg}$ , shown in Fig. 3, which can effectively eliminate the resonant transition background and thus make the spectral peaks more obvious.

$$A(\omega) = \exp\left\{-\frac{(\omega - \omega_0)^2}{2\Delta^2}\right\} \left[1 - \exp\left\{-\frac{(\omega - \omega_{ag})^2}{2\Delta_{hole}^2}\right\}\right] \times \left[1 - \exp\left\{-\frac{(\omega - \omega_{bg})^2}{2\Delta_{hole}^2}\right\}\right], \quad (11)$$

where  $\Delta \gg \Delta_{hole}$ .

We give some pulse shaping methods based on the use of linear and  $\pi$ -step phase-shaping.

$$\phi(\omega) = \phi_L(\omega) + \Theta(\omega), \quad (12)$$

$$\phi_L(\omega) = \begin{cases} k_{d_1}(\omega - \omega_0) & \omega \in (\omega_0, \omega_{fo}) \\ k_{d_2}(\omega - \omega_{fo}) & \omega \in (\omega_{fo}, +\infty), \end{cases} \quad (13)$$

$$\Theta(\omega) = \begin{cases} -\frac{\pi}{2} & \omega \in (\omega_0, \omega_{fb}) \cup (\omega_{fo}, \omega_{fa}) \\ +\frac{\pi}{2} & \omega \in (\omega_{fb}, \omega_{fo}) \cup (\omega_{fa}, +\infty) \end{cases}, \quad (14)$$

where  $\phi(\omega)$  is a linear function and  $\Theta(\omega)$  is a  $\pi$ -step function.

Three phase-shaping schemes are listed for comparison in the following.

- 1) Scheme A uses the transform limited pulse:  $\phi(\omega) = 0$ ,  $\omega \in (\omega_0, \infty)$ ;
- 2) Scheme B is single linear shaping scheme:  $k_{d_1} = k_{d_2}$ ;
- 3) Scheme C is double linear shaping scheme:  $k_{d_1} \neq k_{d_2}$ .

Without loss of generality, we assume  $\phi(\omega) = 0$  when  $\omega \in (-\infty, \omega_0)$ . Here  $\Theta(\omega)$  is a  $\pi$ -step function to compensate the sign change of  $f(\omega)$ , shown in Fig 4(a). And  $\phi_L(\omega)$  is linear function with slopes  $k_{d_1}$  and  $k_{d_2}$ , shown in Fig

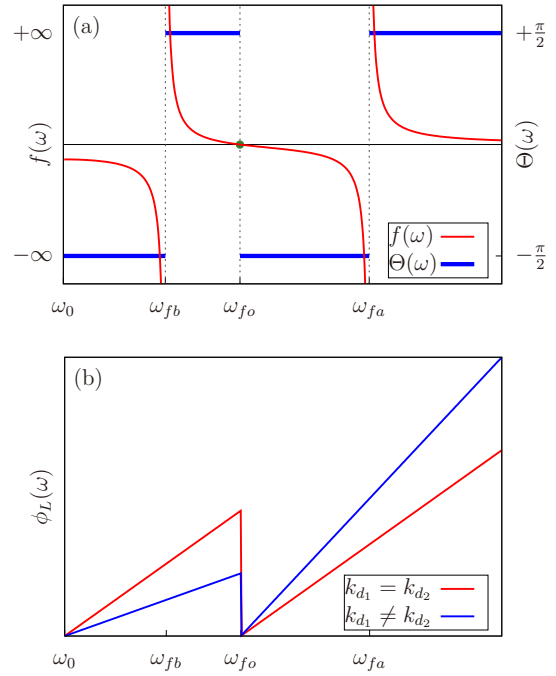


Figure 4: (Color online) The phase shaping schemes. Here  $\Theta(\omega)$  and  $\phi_L(\omega)$  is 0 when  $\omega \in (-\infty, \omega_0)$  (not shown). (a) The step function  $\Theta(\omega)$  is around characteristic frequencies where  $f(\omega)$  changes its sign. (b) The linear function  $\phi_L(\omega)$  with  $k_{d_1} = k_{d_2}$  and  $k_{d_1} \neq k_{d_2}$ .

4(b), which generate local extrema at positions  $k_{d_1}c/2$  and  $k_{d_2}c/2$  via resonance enhancement. In these schemes, only scheme C can achieve effective pathway distinction.

The numerical simulations are shown in Fig. 5. With the scheme A, there is no significant information, except for the enhancement around  $z = 0$ , shown in Fig. 5(a). In the scheme B, the single linear function  $k_{d_1} = k_{d_2}$  leads to the enhancement at position  $k_{d_1}c/2 = 400 \mu\text{m}$ , shown in Fig. 5(b). In the inset of Fig. 5(b), the two pathway amplitudes overlap at  $400 \mu\text{m}$ .

In our distinction scheme C, there are two local extrema at  $k_{d_1}c/2 = 200 \mu\text{m}$  and  $k_{d_2}c/2 = 600 \mu\text{m}$ , shown in Fig. 5(c). The two peak positions are resulted from the linear functions  $k_{d_1}(\omega - \omega_0)$  and  $k_{d_2}(\omega - \omega_{fo})$ , respectively. Pathway 2 dominate the two-photon transitions at the position  $k_{d_1}c/2$ , and pathway 1 dominate at  $k_{d_2}c/2$ . The two-photon transitions  $|U^{(b)}(z)|^2$  at  $200 \mu\text{m}$  and  $|U^{(a)}(z)|^2$  at  $600 \mu\text{m}$  in scheme C are, respectively, approximately equal to  $|U^{(b)}(z)|^2$  and  $|U^{(a)}(z)|^2$  at  $400 \mu\text{m}$  in scheme B. In other words, scheme C could distinguish the two different transition pathways by making them scatter at different positions with double linear functions.

### 4 Conclusion

The spatial coherent control of TPA pathways in atomic rubidium is performed using the counter-propagating ultra-short pulse pairs. A special scheme containing a  $\pi$ -step function and double segmented linear functions is designed to distinguish the two pathways in space. The  $\pi$ -step function part flips the sign at the poles and zeros of the transition amplitude function to make constructive interference between

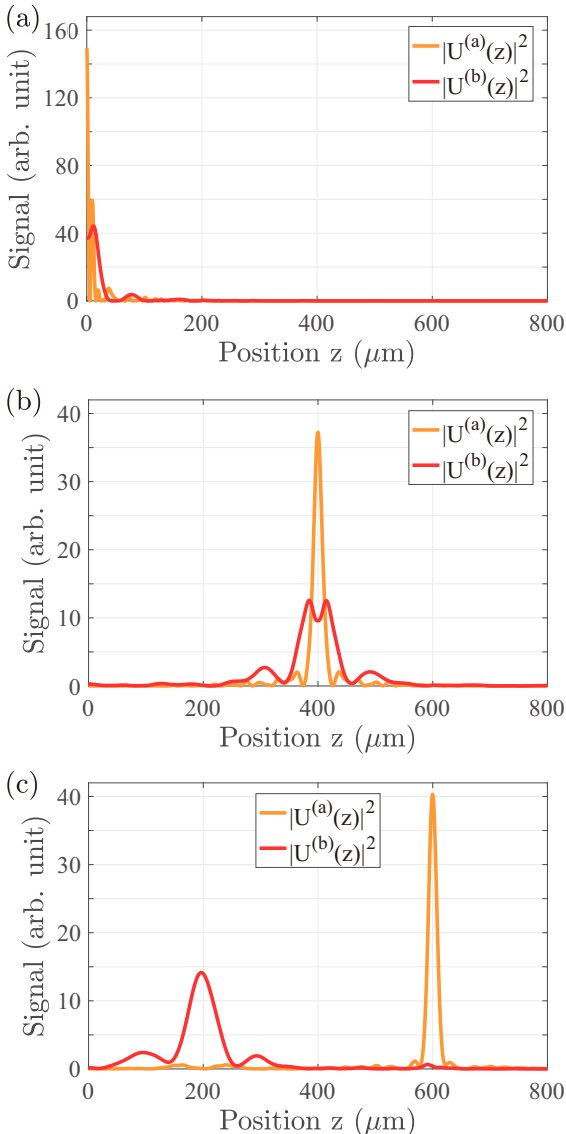


Figure 5: (Color online) The numerical simulations with different phase-shaping schemes. (a) The transform limited pulse (scheme A). (b) Single linear shaping scheme (scheme B) with  $k_{d_1} = k_{d_2} = 2.67$  ps. (c) Double linear shaping scheme (scheme C) with  $k_{d_1} = 1.33$  ps and  $k_{d_2} = 4.00$  ps. Here  $|U(z)|^2$  is proportional to the fluorescence imaged by the CCD. And  $|U^{(n)}(z)|^2$  ( $n = a, b$ ) is the TPA contribution of each transition pathway. As  $U(z)$  and  $U^{(n)}(z)$  are symmetric around  $z = 0$ , only the part of  $z > 0$  is shown.

the two pathways. Meanwhile, the slope of each segmented linear function determines the position of the local excited extrema. The numerical simulations also demonstrate the effectiveness of pathway distinction. This scheme also can be extended to distinguish multiple two-photon transition pathways.

## References

- [1] A. M. Weiner, “Femtosecond pulse shaping using spatial light modulators,” *Review of Scientific Instruments*, vol. 71, no. 5, pp. 1929–1960, 2000.
- [2] D. Meshulach and Y. Silberberg, “Coherent quantum control of two-photon transitions by a femtosecond laser pulse,” *Nature*, vol. 396, no. 6708, pp. 239–242, 1998.
- [3] N. Dudovich, B. Dayan, S. M. Gallagher Faeder, and Y. Silberberg, “Transform-limited pulses are not optimal for resonant multiphoton transitions,” *Phys. Rev. Lett.*, vol. 86, pp. 47–50, Jan 2001.
- [4] S. Zhang, S. Xu, J. Ding, C. Lu, T. Jia, J. Qiu, and Z. Sun, “Single and two-photon fluorescence control of er<sup>3+</sup> ions by phase-shaped femtosecond laser pulse,” *Applied Physics Letters*, vol. 104, no. 1, 2014.
- [5] W. Cheng, S. Zhang, T. Jia, J. Ma, and Z. Sun, “Quantum coherent control of blue, green and red emissions from codoped lanthanide ions of er<sup>3+</sup> tm<sup>3+</sup> yb<sup>3+</sup> by two shaped infrared ultrashort laser beams,” *Laser Physics*, vol. 24, no. 1, p. 015402, 2014.
- [6] Y. Yao, S. Zhang, H. Zhang, J. Ding, T. Jia, J. Qiu, and Z. Sun, “Laser polarization and phase control of up-conversion fluorescence in rare-earth ions,” *Scientific reports*, vol. 4, 2014.
- [7] H.-g. Lee, H. Kim, J. Lim, and J. Ahn, “Quantum interference control of a four-level diamond-configuration quantum system,” *Phys. Rev. A*, vol. 88, p. 053427, Nov 2013.
- [8] F. Gao, R. Rey-de Castro, A. M. Donovan, J. Xu, Y. Wang, H. Rabitz, and F. Shuang, “Pathway dynamics in the optimal quantum control of rubidium: Cooperation and competition,” *Phys. Rev. A*, vol. 89, p. 023416, Feb 2014.
- [9] F. Gao, Y. Wang, R. Rey-de Castro, H. Rabitz, and F. Shuang, “Quantum control and pathway manipulation in rubidium,” *Phys. Rev. A*, vol. 92, p. 033423, Sep 2015.
- [10] D. Cao, L. Yang, Y. Wang, F. Shuang, and F. Gao, “Controlling pathway dynamics of a four-level quantum system with pulse shaping,” *Journal of Physics A: Mathematical and Theoretical*, vol. 49, no. 28, p. 285302, 2016.
- [11] J. Wu, D. Hou, Z. Qin, X. Dai, Z. Zhang, and J. Zhao, “Erbium fiber laser-based direct frequency comb spectroscopy of rb two-photon transitions,” *Opt. Lett.*, vol. 38, pp. 5028–5031, Dec 2013.
- [12] W. Xia and X. Chen, “Recent developments in fiber-based optical frequency comb and its applications,” *Measurement Science and Technology*, vol. 27, no. 4, p. 041001, 2016.
- [13] W.-B. Dong, R.-B. Wu, W. Zhang, C.-W. Li, and T.-J. Tarn, “Spatial control model and analysis of quantum fields in one-dimensional waveguides,” *SIAM Journal on Control and Optimization*, vol. 54, no. 3, pp. 1352–1377, 2016.
- [14] I. Barmes, S. Witte, and K. S. Eikema, “Spatial and spectral coherent control with frequency combs,” *Nature Photonics*, vol. 7, pp. 38–42, Dec 2013.
- [15] I. Barmes, S. Witte, and K. S. Eikema, “High-precision spectroscopy with counterpropagating femtosecond pulses,” *Phys. Rev. Lett.*, vol. 111, p. 023007, Jul 2013.
- [16] D. Boonzajer, *Coherent control of two-photon transitions in Rubidium*. mathesis, University of Amsterdam, Nov. 2013.
- [17] W. Lee, H. Kim, K. Kim, and J. Ahn, “Coherent control of resonant two-photon transitions by counterpropagating ultrashort pulse pairs,” *Phys. Rev. A*, vol. 92, p. 033415, Sep 2015.